MOLECULAR
METABOLISM

De novo labeling and trafficking of individual lipid species in live cells

Jun Zhang [1,2,4], Jia Nie [1,4], Haoran Sun [3,4], Jie Li [3], John-Paul Andersen [1], Yuguang Shi [1,3,*]

ABSTRACT

Objective: Lipids exert dynamic biological functions which are determined both by their fatty acyl compositions and spatiotemporal distributions inside the cell. However, it remains a daunting task to investigate any of these features for each of the more than 1000 lipid species due to a lack of a universal labeling method for individual lipid moieties in live cells. Here we report a *de novo* lipid labeling method for individual lipid species with precise acyl compositions in live cells. The method is based on the principle of *de novo* lipid remodeling of exogenously added lysolipids with fluorescent acyl-CoA, leading to the re-synthesis of fluorescence-labeled lipids which can be imaged by confocal microscopy.
Methods: The cells were incubated with lysolipids and a nitro-benzoxadiazolyl (NBD) labeled acyl-CoA. The newly remodeled NBD-labeled lipids and their subcellular localization were analyzed by confocal imaging in live cells. Thin layer chromatography was carried out to verify the synthesis of NBD-labeled lipids. The mitochondrial trafficking of NBD-labeled lipids was validated in live cells with targeted deletion of phospholipids transporters, including TRIAP1/PRELI protein complex and StarD7.
Results: Incubation cells with lysolipids and NBD-acyl-CoA successfully labeled major lipid species with precise acyl compositions, including phospholipids, cholesterol esters, and neutral lipids, which can be analyzed by confocal imaging in live cells. In contrast to exogenously labeled lipids, the *de novo* labeled lipids retained full biological properties of their endogenous counterparts, including subcellular localization, trafficking, and recognition by lipid transporters. This method also uncovered some unexpected features of newly remodeled lipids and their transporters.
Conclusions: The *de novo* lipid labeling method not only provides a powerful tool for functional analysis of individual lipid species and lipid transporters, but also calls for re-evaluation of previously published results using exogenously labeled lipids.

1. INTRODUCTION

Eukaryotic cells contain thousands of different lipid species which are classified into seven categories according to their fatty acyl structures and pathways of biosynthesis, including glycerol lipids, phospholipids, sterol lipids, sphingolipids, prenol lipids, and saccharolipids [1]. Lipids are highly organized within eukaryotic cells with diversified biological activities, such as membrane structure, energy storage, signal transduction, autophagy, epigenetic modifications, and vesicular trafficking [2]. The precise function of an individual lipid is determined by both its acyl composition and subcellular localization. However, in contrast to DNA and proteins, there is a lack of a universal labeling method for individual lipid species, which makes it very difficult to investigate the spatiotemporal distribution of a given lipid molecule and to answer the key question as to when a lipid molecule performs each of its functions within a live cell.

Although various attempts have been made in recent years to investigate subcellular localization and trafficking of lipids by microscopic visualization in live cells [2–4], it has been met with limited success to date due to a lack of lipid species-specific labeling of endogenous lipids. Consequently, most lipid trafficking studies reported to date relied heavily on the use of exogenously labeled lipids or nonspecific fluorescent labeling, such as BODIPY for neutral lipids and Filipin for cholesterol, which renders the results difficult to interpret. BODIPY labels endogenous neutral lipids and phospholipids without any specificity for acyl composition, whereas fluorophore-conjugated lipids do not mimic the biological functions of the endogenous counterparts, since most of them are subjected to lysosomal degradation after endocytic uptake [5]. In addition, none of the existing lipid labeling methods can be used to monitor the subcellular localization and trafficking of endogenous lipids. In this study, we resolved these issues by developing a *de novo* lipid labeling method which can be used for confocal imaging analysis of precise

[1]Sam and Ann Barshop Institute for Longevity and Aging Studies, Department of Pharmacology, University of Texas Health Science Center at San Antonio, 4939 Charles Katz Drive, San Antonio, TX, 78229, USA [2]Perenna Pharmceuticals Inc., 14785 Omicron Drive, Ste 100, San Antonio, TX, 78245, USA [3]Department of Biochemistry and Molecular Biology, Nanjing Medical University, Nanjing, People's Republic of China

[4] These authors contributed equally to the work.

*Corresponding author. Joe R. & Teresa Lozano Long Distinguished Chair in Metabolic Biology, Professor of Pharmacology, Barshop Institute for Longevity and Aging Studies, University of Texas Health Science Center at San Antonio, 4939 Charles Katz Drive, San Antonio, TX 78229. fax: +210 562 6150. E-mail: shiy4@uthscsa.edu (Y. Shi).

Original Article

subcellular localization and trafficking of individual lipid species in live cells. The method is based on the principle that all lipid species undergo a periodical remodeling process after initial synthesis to achieve appropriate acyl contents or to repair damaged acyl chains from oxidative stress [6]. The remodeling process, also known as the Lands cycle, mainly takes place both at the endoplasmic reticulum (ER)—mitochondrial junctions and lipid droplets (LDs), and is catalyzed by a superfamily of lipases and acyltransferases [7—9]. We show in this study that the remodeling process provides a unique opportunity to label individual species by feeding the cultured cells with individual lysolipids or lysophospholipids and a nitro-benzoxadiazolyl (NBD, a fluorescent probe) labeled acyl-CoA (NBD-acyl-CoA) with predesignated acyl composition. The lysolipids and lysophospholipids are re-acylated at the sn-2 position, which is catalyzed by the endogenous acyltransferases by using NBD-acyl-CoA as the acyl donor. Incorporation of NBD-labeled fatty acyl chains into newly remodeled lipids and phospholipids generates green fluorescence signal which allows for confocal imaging analysis of the subcellular localization and trafficking of individual lipid species in live cells (Figure 1A). We have successfully applied this method to investigate the subcellular localization and trafficking of major lipid species with precise acyl compositions, including phospholipids, cholesterol esters (CE), and neutral lipids in live cells by confocal imaging analysis.

2. MATERIALS AND METHODS

2.1. Reagents

{N-[(7-nitro-2-1,3-benzoxadiazol-4-yl)-methyl]amino} palmitoyl Coenzyme A (NBD-palmitoyl-CoA, #810705), 1-(9Z-octadecenoyl)-sn-glycero-3-phosphate (LPA 18:1, #857130), 1-(9Z-octadecenoyl)-sn-glycero-3-phosphocholine (LPC 18:1, #845875), 1-(9Z-octadecenoyl)-sn-glycero-3-phosphoethanolamine (LPE 18:1, #846725), 1-(9Z-octadecenoyl)-sn-glycero-3-phospho-(1′-sn-glycerol) (LPG 18:1, #858125), 1'-[1-(9Z,12Z-octadecadienoyl)-sn-glycero-3-phospho],3'-[1,2-di-(9Z,12Z-octadecadienoyl)-sn-glycero-3-phospho]-sn-glycerol (MLCL, CL 54:6, #850081), 1-oleoyl-2-{12-[(7-nitro-2-1,3-benzoxadiazol-4-yl)amino]dodecanoyl}-sn-glycero-3-phosphate (18:1—12:0 NBD-PA, #810176), 1-oleoyl-2-{12-[(7-nitro-2-1,3-benzoxadiazol-4-yl)amino]dodecanoyl}-sn-glycero-3-phosphoserine (18:1—12:0 NBD-PS, #810195), 1-oleoyl-2-{12-[(7-nitro-2-1,3-benzoxadiazol-4-yl)amino]dodecanoyl}-sn-glycero-3-[phospho-rac-(1-glycerol)] (18:1—12:0 NBD-PG, #810166), 1-oleoyl-2-[12-[(7-nitro-2-1,3-benzoxadiazol-4-yl)amino]dodecanoyl]-sn-glycero-3-phosphocholine (18:1—12:0 NBD-PC, #810133), and 25-[N-[(7-nitro-2-1,3-benzoxadiazol-4-yl)methyl]amino]-27-norcholesterol (25-NBD-Cholesterol, #810250) were purchased from Avanti Polar Lipids. Palmitoyl coenzyme A lithium salt (#P9716), Cholesterol (#C3045), 1,2-di-(9Z-octadecenoyl)-sn-glycerol (DG 36:2, #D0138), 2-(9Z-octadecenoyl)-sn-glycerol (MG 18:1, #M2787), Avasimibe (#PZ0190), methyl-β-cyclodextrin (MCD, #C4555), Etomoxir (#E1905), and thin-layer chromatography (TLC) plates (#60805) were from Sigma. MitoTracker Red CMXRos (#M7512), LysoTracker™ Red DND-99 (#L7528), and BODIPY™ 650/665-X NHS Ester (#D10001) were from ThermoFisher Scientific. Mito-BFP (#49151) and DsRed2-ER5 (#55836) were from Addgene.

2.2. Generation of gene knockout cells using CRISPR-Cas9 gene editing

Triap1, Prelid1 and Stard7 genes were knocked out in C2C12 cells by transfecting CRISPR-Cas9 mouse plasmids from Santa Cruz using Viafect Transfection Reagent (#E4982, Promega), and then purified through GFP and RFP fluorescence by the UT Health San Antonio Flow Cytometry Core. Cells were then kept under selection with 10 μg/mL puromycin (#sc-205821, Santa Cruz). Vector control cells were created by transfecting C2C12 cells with an empty pBABE-puro vector backbone (#1764, Addgene) and selected and kept in culture medium with 10 μg/mL puromycin. The efficiency of gene knockout was confirmed by quantitative real-time PCR (qRT-PCR) analysis.

2.3. Lactate dehydrogenase (LDH) assay

The cells were first nutrient starved in a standard Krebs Ringer Phosphate HEPES buffer (KRPH, 140 mM NaCl, 2 mM Na_2HPO_4, 4 mM KCl, 1 mM $MgCl_2$, 1.5 mM $CaCl_2$, 10 mM HEPES, pH7.4) for 1 h and then incubated with NBD-palmitoyl-CoA (1 μM) alone or plus indicated concentrations of lysophospholipids in KRPH buffer for 1 h. The cell viability was determined by using the LDH cytotoxicity assay kit (#PI88953, Thermo Scientific) according to the manufacturers' instruction.

2.4. Live cell fluorescence labeling and confocal microscopic settings

Cells were plated on 35 mm glass bottom dishes for live cell confocal imaging analysis. Cells were transfected with DsRed2-ER5 to label the ER, and stained with MitoTracker Red (50 nM) in complete medium (CM) for 15 min to label mitochondria. Lysosomes were stained with LysoTracker Red (100 nM). To visualize lipid droplets, cells were stained with BODIPY 650/665-X NHS Ester for 1 h. Nuclei were stained by Hoechst 33342 (Invitrogen). Images were taken using a Zeiss LSM 710 confocal microscope with Zeiss Plan Apochromat 63x/1.4 oil objective. The confocal microscopic settings for each fluorescent dye are shown in Table 1.

### 2.5. Labeling of newly remodeled phospholipids in cells

C2C12 or COS-7 cells were cultured in DMEM with 10% FBS and 1% penicillin/streptomycin. For lipid labeling, cells were first nutrient starved in KRPH buffer for 1 h and then incubated with NBD-palmitoyl-CoA (1 μM) and lysophospholipids (20 μM for LPG 18:1, 50 μM for MLCL, LPA 18:1, and LPC 18:1) in KRPH buffer for 10—15 min. For visualizing of mitochondria, cells were stained with MitoTracker Red before nutrient starvation in CM for 15 min. For visualizing the ER, cells were transfected with DsRed2-ER5. Images were taken using a Zeiss LSM 710 confocal microscope with the settings shown in Table 1.

2.6. Labeling of newly remodeled CE in cells

For labeling the newly remodeled CE, C2C12 cells were first pre-treated with 0.5% methyl-beta cyclodextrin (MCD) in DMEM supplemented with 0.5% fatty acid free BSA (#700—107P, Gemini) for 2 h. Cells were then incubated with NBD-palmitoyl-CoA (1 μM) alone or plus cholesterol (50 μM) which was pre-complexed with 0.1% MCD in DMEM supplemented with 0.5% fatty acid free BSA for 30 min. For visualizing of mitochondria, cells were stained with MitoTracker Red before MCD treatment in CM for 15 min. To inhibit the acylation of cholesterol in cells, C2C12 cells were pre-treated with avasimibe (10 μM), a selective inhibitor of acyl-CoA:cholesterol acyltransferases, for 4 h in CM, and then subjected to mitochondrial staining and cholesterol labeling. Images were taken using a Zeiss LSM 710 confocal microscope with the settings shown in Table 1.

2.7. Labeling of newly synthesized triacylglycerol (TG) in cells

COS-7 cells were transfected with DsRed2-ER5 to visualize the ER. After 36—48 h of transfection, cells were first nutrient starved in
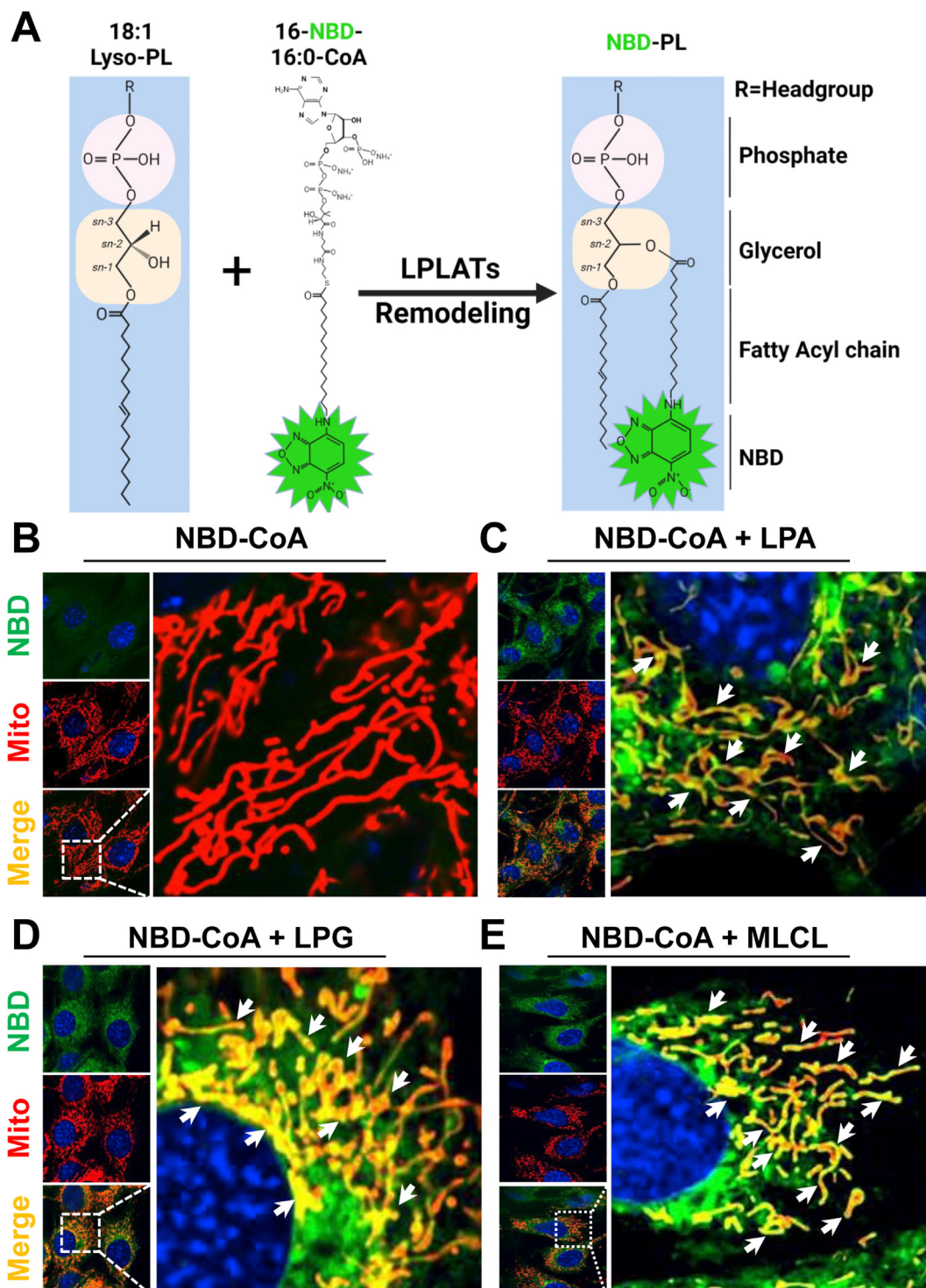
Figure 1: *De novo* labeling and confocal imaging of phospholipids in live cells. (**A**) Schematic representation of *de novo* lipid labeling in live cells supplemented with 16-NBD 16:0-CoA and 18:1 lysophospholipids (Lyso-PL) by the endogenous lipid remodeling pathways. LPLATs, lysophospholipids acyltransferases. (**B-E**) Confocal imaging analysis of newly remodeled and NBD-labeled phospholipids in live C2C12 cells. C2C12 cells were incubated with NBD-palmitoyl-CoA (1 μM) alone (**B**), or NBD-palmitoyl-CoA plus LPA 18:1 (50 μM) (**C**), LPG 18:1 (20 μM) (**D**), or MLCL (50 μM) (**E**). Mitochondria were stained with MitoTracker Red. Arrows highlight the co-localization of NBD-PL (green) with mitochondria (red). Data are representative of at least three independent experiments.

Table 1 — Confocal microscopic settings of fluorescent dyes.

Dye	Laser/ nm	Laser Power	Emission range/nm	Gain	Digital Gain	Bit Depth	Frame Size
NBD	488	2.0	490—560	700	1.0	12	1024 × 1024
MitoTracker Red	561	5.0	574—630	850	1.0	12	1024 × 1024
DsRed	561	5.0	566—630	800	1.0	12	1024 × 1024
Hoechst 33342	405	2.0	410—484	700	1.0	12	1024 × 1024
BODIPY™ 650/665	633	5.0	637—730	800	1.0	12	1024 × 1024
LysoTracker Red	561	5.0	580—691	800	1.0	12	1024 × 1024

KRPH buffer for 1 h, and then incubated with NBD-palmitoyl-CoA (1 μM) and DG 36:2 (25 μM) or MG 18:1 (25 μM) in KRPH for 10—15 min. To observe the co-localization of the newly synthesized TG with lipid droplets, cells were first stained with BODIPY 650/665-X NHS Ester in KRPH buffer for 1 h during the nutrient starvation. Cells were washed twice with KRPH buffer, and then subjected to incubation with NBD-palmitoyl-CoA and DG 36:2 or MG 18:1. To inhibit the DGAT1 activity, cells were pre-treated with A922500 (10 μM) for 1 h, followed by incubation with NBD-palmitoyl-CoA and DG 36:2. Images were taken using a Zeiss LSM 710 confocal microscope with the settings shown in Table 1.

2.8. Quantification of the co-localization of NBD with mitochondria
Pearson's correlation coefficient was used for the co-localization analysis of NBD signaling with mitochondria. The ImageJ software with a JACoP plugin was used for the Pearson's correlation coefficient analysis [10]. In brief, images of individual cells were first split to blue, green and red channels, and the Pearson's correlation coefficient of green channel (NBD) and red channel (Mitochondria) was analyzed by using JACoP plugin. Identical settings were used to analyze at least 20 cells per condition.

2.9. Measurement of free cholesterol contents
C2C12 cells were first pre-treated with 0.5% MCD in DMEM supplemented with 0.5% fatty acid free BSA for 2 h. The control cells were starved in DMEM supplemented with 0.5% fatty acid free BSA for 2 h. To inhibit the acylation of cholesterol in cells, C2C12 cells were first treated with avasimibe (10 μM) for 4 h in CM before MCD treatment. Cells were then incubated with palmitoyl-CoA (1 μM) alone or plus cholesterol (50 μM) which was pre-complexed with 0.1% MCD in DMEM supplemented with 0.5% fatty acid free BSA for 30 min. Cells were then harvested, and the free cholesterol contents were measured using the Cholesterol/Cholesterol Ester-Glo Assay Kit (#J3190, Promega) according to the manufacturer's instructions.

2.10. Lipids extraction and TLC analysis
To confirm the remodeled or newly synthesized lipid products, cells were incubated with NBD-palmitoyl-CoA and different lysophospholipids, cholesterol, DG 36:2 or MG 18:1 as described above. Mitochondria was isolated and purified according to the method described previously [11]. Total lipids from total cells or isolated mitochondria were extracted using chloroform/methanol (2:1, v/v). The lipid samples were loaded to a TLC plate (Sigma), and developed in the following solvent mixtures: chloroform: ethanol: water: trimethylamine (30:35:7:35, v/v/v/v) for phosphatidic acid (PA), chloroform: methanol: water (65:25:4, v/v/v) for glycerophosphocholine (PC) and glycerophosphoglycerol (PG), and

hexane: diethyl ether: acetic acid (70:30:1, v/v/v) for CE. For development of TG, the lipid samples were loaded to the TLC plate which was first migrated in chloroform/methanol (1/1, v/v), and developed in the solvent mixture: hexane: diethyl ether: acetic acid (70/30/1, v/v/v). The lipid samples from cells only incubated with NBD-palmitoyl-CoA was loaded as a negative control. The in vitro NBD labeled phospholipids were used as lipids markers. The TLC plates were dried after development and scanned using a Typhoon 9410 Scanner.

2.11. Lipidomic analysis
The lipidomic analysis was carried out using methods previously described [6]. Briefly, total lipids extracted from cells incubated with NBD-palmitoyl-CoA alone or plus LPG were analyzed by triple-quadruple mass spectrometer (MS) (Thermo Electron TSQ Quantum Ultra) controlled by Xcalibur system software. All the MS spectra and tandem MS spectra were automatically acquired by a customized sequence subroutine operated under Xcalibur software.

2.12. Visualizing of in vitro NBD labeled lipids in cells
To observe subcellular localization of the in vitro NBD labeled lipids in cells, C2C12 cells were first nutrient starved in KRPH buffer for 1 h, and then incubated with in vitro NBD labeled lipids (1 μM), including NBD-PA, NBD-PC, and NBD-PS for 15 min in KRPH buffer. For NBD-cholesterol, cells were first pre-treated with 0.5% MCD in DMEM supplemented with 0.5% fatty acid free BSA for 2 h, and then incubated with NBD-cholesterol (1 μM) pre-complexed with 0.1% MCD in DMEM supplemented with 0.5% fatty acid free BSA for 30 min. Lysosomes were stained with LysoTracker Red. Images were taken using a Zeiss LSM 710 confocal microscope with the settings shown in Table 1.

### 2.13. Quantification and statistical analysis
Data were routinely represented as mean $\pm$ SD. Statistical significance was assessed by unpaired Student's t test or one-way ANOVA using GraphPad Prism 7.0. Differences were considered statistically significant at $p < 0.05$; *$p < 0.05$; **$p < 0.01$; ***$p < 0.001$.

3. RESULTS

3.1. A de novo lipid labeling method of individual phospholipid species with precise acyl composition in live cells
Lipid remodeling is a widespread strategy after the initial synthesis by the Kennedy pathway, which plays a critical role in maintaining appropriate acyl composition of a given lipid species. The remodeling process begins with hydrolysis of fatty acyl chains, followed by re-acylation with the required fatty acid, which is catalyzed by a family of acyltransferases using acyl-CoA as the acyl donor (Figure 1A). We questioned whether the remodeling process could provide an opportunity for de novo labeling of individual lipid species with pre-determined acyl composition by culturing the cells with NBD-acyl-CoAs and lysophospholipids, leading to the production of NBD-labeled phospholipids. Due to the attachment of NBD which is a fluorescent probe, the newly remodeled phospholipids can be imaged in live cells by confocal microscopy.

We first tested this hypothesis for the de novo labeling of PA in C2C12 cells, a skeletal myocyte cell line. PA is a precursor for the synthesis of all the phospholipids, including PC, glycerophosphoethanolamine (PE), glycerophosphoserine (PS), glycerophosphoinositol (PI), PG, and cardiolipin (CL). C2C12 cells were stained with MitoTracker Red, a mitochondrial specific fluorescent dye, and cultured in the presence of either NBD-palmitoyl-CoA alone or in the presence of LPA 18:1, a substrate for
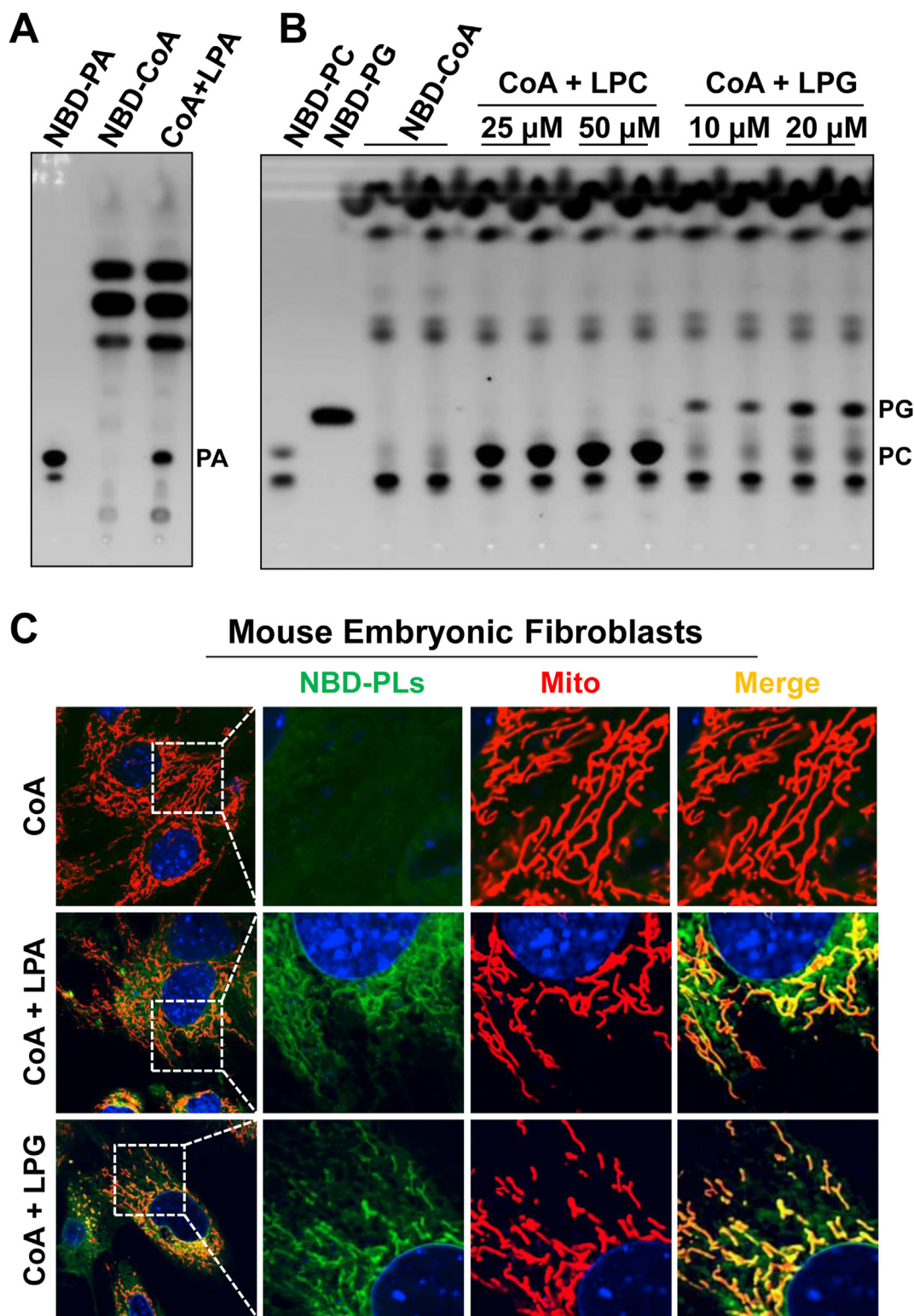
Figure 2: Analysis of NBD labeled phospholipids by TLC and in primary MEFs by confocal imaging analysis. (A) TLC analysis of newly remodeled PA in C2C12 cells. **(B)** TLC analysis of newly remodeled PC and PG in C2C12 cells. Cells were starved in KRPH buffer for 1 h, and then incubated with NBD-palmitoyl-CoA alone or with LPA 18:1 (50 μM), LPC 18:1 (25 μM and 50 μM) or LPG 18:1 (10 μM and 20 μM) for 15 min, respectively. *In vitro* labeled 18:1—12:0 NBD-PA, 18:1—12:0 NBD-PC, and 18:1—12:0 NBD-PG were used as standards. **(C)** Labeling and confocal imaging of phospholipids in live primary MEFs. Primary MEFs were starved in KRPH buffer for 1 h, and then incubated with NBD-palmitoyl-CoA (1 μM) alone or NBD-palmitoyl-CoA plus LPA 18:1 (50 μM) or LPG 18:1 (20 μM) for 15 min. Mitochondria were stained with MitoTracker Red. Data are representative of at least three independent experiments.

PA synthesis. No significant green fluorescence signal was detected in cells cultured with NBD-palmitoyl-CoA alone (Figure 1B). In contrast, supplementation of culturing medium with both NBD-palmitoyl-CoA and LPA 18:1 resulted in detection of strong green fluorescent signals (Figure 1C), suggesting specific labeling of newly remodeled PA. PA is primarily remodeled in the ER, and is transported to mitochondria where it is used as the precursor for the synthesis of mitochondrial specific phospholipids, including PG and CL. Consistent with this notion, most of the newly labeled PA appeared in mitochondria, as evidenced by co-localization of red (mitochondria) and green (PA) fluorescence that resulted in yellow color (Figure 1C, highlighted by arrows), and by results from time-lapse confocal imaging analysis (Fig. S1). In support of the versatility of the labeling method, incubation of C2C12 cells with NBD-palmitoyl-CoA in the presence of LPG 18:1 or monolysocardiolipin (MLCL, CL 54:6), the substrates for the remodeling of PG and CL, respectively. Both PG and CL are mitochondrial phospholipids that are rapidly transported to mitochondria after remodeling, as evidenced by the presence of yellow fluorescent color (Figure 1D—E, highlighted by arrows). In contrast to PG and CL which are exclusively localized in mitochondria after remodeling (Figs. S2 and S3, highlighted by arrows), only part of the newly remodeled PC was transported to mitochondria, as supported by results from time-lapse confocal imaging analysis (Figure 4, arrows highlight the co-localization of NBD-PC with mitochondria (Fig. S4A) or the ER (Fig. S4B), respectively), suggesting that attachment of NBD to the phospholipids did not abolish their recognition by mitochondrial phospholipid transporters.

One of the major concerns for the labeling method is whether these exogenous lipids, when used at the concentration for *de novo* lipid labeling, would lead to cellular toxicity which would render the results difficult to interpret. To answer this question, we determined the dose-dependent effect of the exogenously added lysophospholipids, including LPA, LPC, LPE, and LPG, on cell viability. The results showed that none of lysophospholipids, including LPA, LPC and LPE, caused cell death at the concentrations lower than 100 μM (Figs. S5A—C). Among all the lysophospholipids, LPG was the most toxic one, which started to cause cell death at 30 μM (Fig. S5D). In contrast, none of the lysophospholipids, including LPA, LPC, LPG, MLCL, and cholesterol, exhibited significant cellular toxicity at concentrations used for the *de novo* lipid labeling method (50 μM for LPA, MLCL, LPC and cholesterol; and 20 μM for LPG, Fig. S5E). Consistent with the findings, none of the lysophospholipids caused ER stress or mitochondrial fragmentation in cells when used at the same concentration as in the *de novo* lipid labeling method, as evidenced by results from western blot analysis of major ER stress biomarkers, including ATF4 and phosphorylated PERK, as well as key regulators of the mitochondrial fusion and fission process, including phosphorylated DRP1, MFN2, and OPA1 (Fig. S5F). Additionally, neither LPA nor MLCL affected the mitochondrial respiration, as shown by seahorse analysis of mitochondrial oxygen consumption rate (OCR) (Figs. S5G—H). Although LPG incubation slightly decreased the ATP-linked OCR and the spare capacity, it did not affect the basal and maximal OCRs (Figs. S5G—H).

We next addressed other possible concerns arising from the labeling method, including the identity of the remodeled phospholipids, specificity of the labeling method, and possibility of further modifications after the initial remodeling. Using TLC analysis, we addressed these important concerns by validating whether the fluorescent signals we detected from the live C2C12 cells were indeed generated from the remodeling process, and if so, whether these remodeled lipids were further used for the synthesis of other phospholipids. In further support of the specificity of the labeling, the results showed that NBD-labeled phospholipids, including PA, PG, and PC, can only be detected if both

NBD-palmitoyl-CoA and lysophospholipids were added to the culture medium (Figure 2A—B). Moreover, these newly remodeled phospholipids were not further remodified, as there were no significant increases in other NBD-labeled phospholipid species other than the predesignated phospholipid species. Furthermore, the labeling significantly increased content of PG species with acyl composition that precisely matches that of the LPG, as evidenced by results from lipidomic analysis (Fig. S6). Together, these results further confirm that the *de novo* labeling method is highly specific, and attachment of NBD to newly remodeled phospholipids did not significantly affect their biological activity or lead to cellular toxicity when the lysophospholipids were used at the designated concentrations.

Using isolated mouse embryonic fibroblasts (MEFs) and primary hepatocytes, we determined whether the lipid labeling method could be applied to study subcellular localization and trafficking of phospholipids in primary cells. Consistent with findings from C2C12 cells, incubation of MEFs and primary mouse hepatocytes with both NBD-palmitoyl-CoA and LPA or LPG resulted in NBD-palmitoyl-CoA dependent remodeling of PA or PG, respectively. Again, attachment of NBD to newly remodeled PA and PG did not affect their recognition by mitochondrial phospholipid transporters, which is supported by the observation that NBD-labeled PA and PG were efficiently transported to the mitochondria both in MEFs (Figure 2C) and primary mouse hepatocytes (Fig. S7), suggesting that the labeling method can also be used to study lipid trafficking in primary cells as well.

3.2. *De novo* lipid labeling uncovered novel function of previously identified phospholipid transporters

Currently, analysis of lipid transporter activity is commonly carried out by liposome-based assays *in vitro* using the purified protein to be tested [12]. Though this method provides a tool to investigate the activity of a protein or a protein complex in lipid binding and trafficking *in vitro*, some of the purified proteins, especially the membrane proteins, do not faithfully mimic the endogenous membranous environment, such as the ER and mitochondrial membranes. Additionally, currently there is no method to directly validate the function of a protein in lipid trafficking in live cells. To further validate the specificity and utility of the *de novo* lipid labeling technique, we next determined whether our method can be used to identify lipid transporter activity of a given protein in live cells.

We first tested the function of the TRIAP1/PRELI protein complex which was previously shown to facilitate the mitochondrial PA transport [12]. Using the CRISPR-Cas9 technique, we generated C2C12 stable cell lines with targeted deletion of the *Prelid1* or *Triap1* gene which was confirmed by qRT-PCR analysis (Figs. S8A—B). Consistent with the previously reported function of the complex, ablation of PRELID1 or TRIAP1 in C2C12 cells significantly impaired PA transport from the ER to mitochondria, leading to the ER retention of newly remodeled PA (Figure 3A—C, arrows highlight the co-localization of NBD-PA with mitochondria, quantified by Pearson's correlation coefficient analysis in Figure 3G). The findings are further supported by results from time-lapse confocal imaging analysis in live C2C12 cells stained with MitoTracker Red (Figs. S8C—E). Remarkably, the method also revealed a novel function for PRELID1 in PG transport, which was missed by the conventional liposomal assay [12]. Accordingly, PRELID1 deficiency, but not TRIAP1, significantly impaired the transport of newly remodeled PG to mitochondria (Figure 3D—F, arrows highlight the co-localization of NBD-PG with mitochondria, quantified by Pearson's correlation coefficient of mitochondria and NBD-PG in Figure 3H,I, respectively). This result is corroborated by a previous report that PRELI deficiency, but not TRIAP1, significantly reduced the PG content in mitochondria [12]. In further
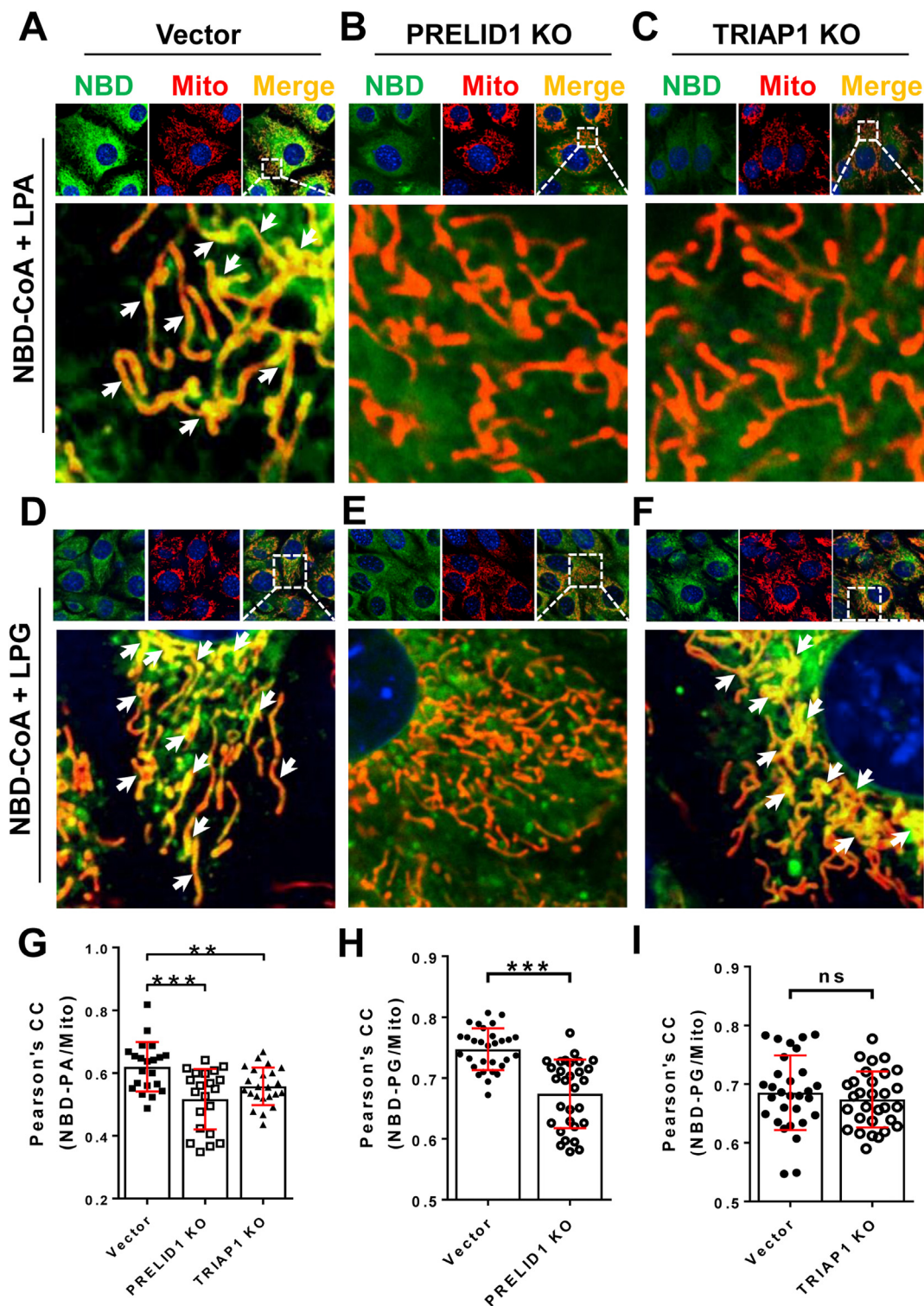
Figure 3: TRIAP/PRELID1 complex is required for mitochondrial PA and PG, but not PC transport. (A-C) Confocal imaging analysis of the NBD labeling and mitochondrial transport of PA in live C2C12 vector control (**A**), PRELID1 knockout (KO) (**B**), and TRIAP1 KO (**C**) cells. Arrows in **A** highlight the co-localization of NBD-PA with mitochondria. (D-F) Confocal imaging analysis of NBD labeling and mitochondrial transport of PG in live C2C12 vector control (**D**), PRELID1 KO (**E**), and TRIAP1 KO (**F**) cells. Arrows in **D** and **F** highlight the co-localization of NBD-PG with mitochondria. (**G**) Pearson's correlation coefficient of NBD-PA and mitochondria in vector, PRELID1 KO, and TRIAP1 KO cells. n = 21−23 cells/ group. (**H**−**I**) Pearson's correlation coefficient of NBD-PG and mitochondria in vector and PRELID1 KO (**H**) or TRIAP1 KO cells (**I**). n = 30 cells/group. Cells were starved in KRPH buffer for 1 h, and then incubated with NBD-palmitoyl-CoA (1 μM) and LPA 18:1 (50 μM) (**A-C**) or LPG 18:1 (20 μM) (**D-F**) for 15 min. Mitochondria were stained with MitoTracker Red. Data are representative of at least three independent experiments, and are represented as mean ± SD, **p < 0.01, ***p < 0.001, ns, no significance by student's t-test.
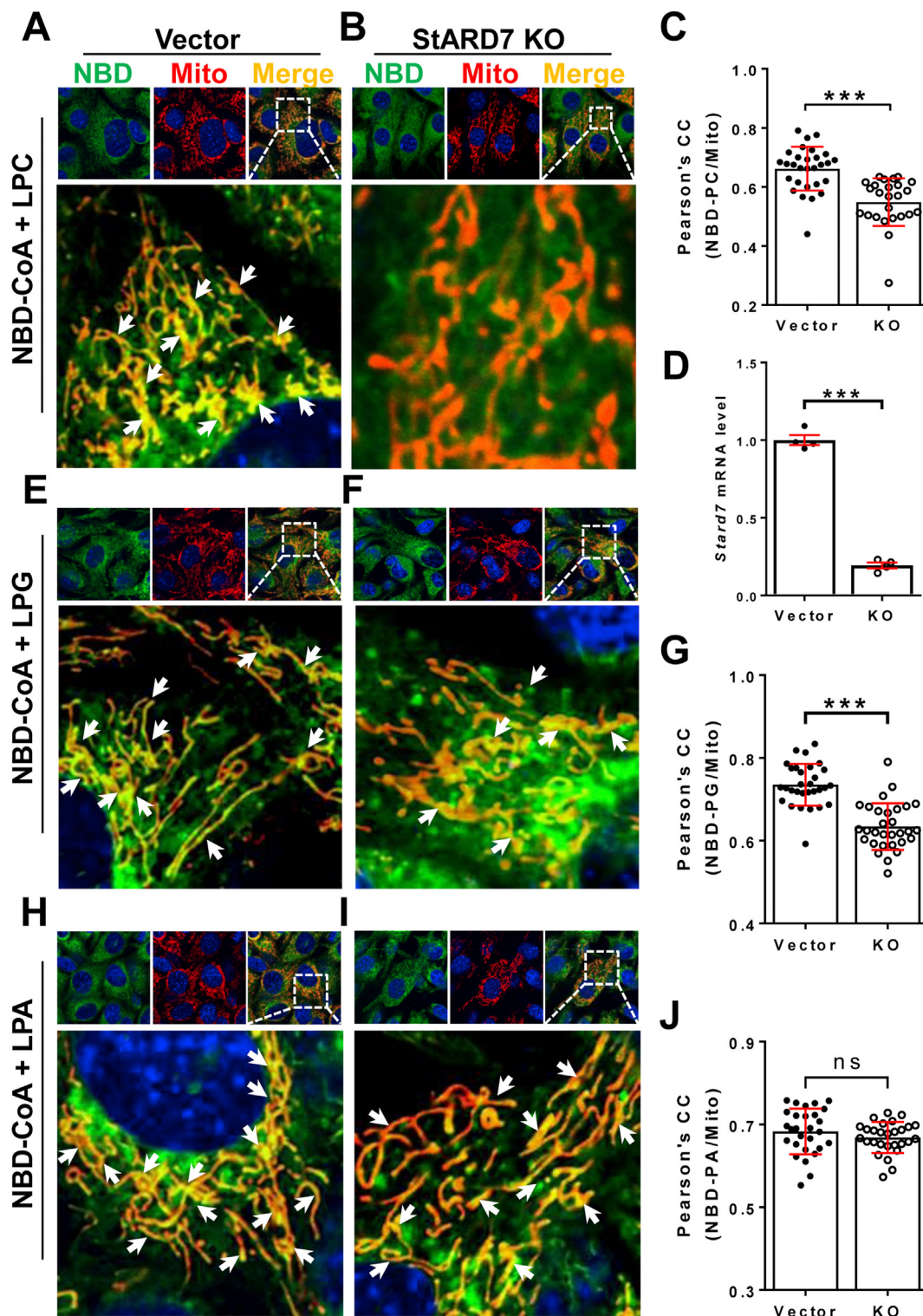
Figure 4: StARD7 is required for mitochondrial PC and PG, but not PA transport. (A-B) Confocal imaging analysis of NBD labeling and mitochondrial transport of PC in live C2C12 vector control (**A**) and StARD7 KO (**B**) cells. Arrows in **A** highlight the co-localization of NBD-PC with mitochondria. (**C**) Pearson's correlation coefficient of NBD-PC and mitochondria in vector and StARD7 KO cells. n = 25−29 cells/group. (**D**) qRT-PCR analysis of *Stard7* mRNA expression in C2C12 vector and StARD7 KO cells. (E-F) Confocal imaging analysis of the labeling and mitochondrial transport of PG in live C2C12 vector control (**E**) and StARD7 KO (**F**) cells. Arrows highlight the co-localization of NBD-PG with mitochondria. (**G**) Pearson's correlation coefficient of NBD-PG and mitochondria in vector and StARD7 KO cells. n = 30 cells/group. (**H−I**) Confocal imaging analysis of NBD labeling and mitochondrial transport of PA in live C2C12 vector control (**H**) and StARD7 KO (**I**) cells. Arrows highlight the co-localization of NBD-PA with mitochondria. (**J**) Pearson's correlation coefficient of NBD-PA and mitochondria in vector and StARD7 KO cells. n = 28 cells/group. Cells were starved in KRPH buffer for 1 h, and then incubated with NBD-palmitoyl-CoA (1 μM) and LPC 18:1 (50 μM) (**A-B**), LPG 18:1 (20 μM) (**E-F**), or LPA 18:1 (50 μM) (**H−I**) for 15 min. Mitochondria were stained with MitoTracker Red. Data are representative of at least three independent experiments, and are represented as mean ± SD, ***$p < 0.001$, ns, no significance by student's t-test.
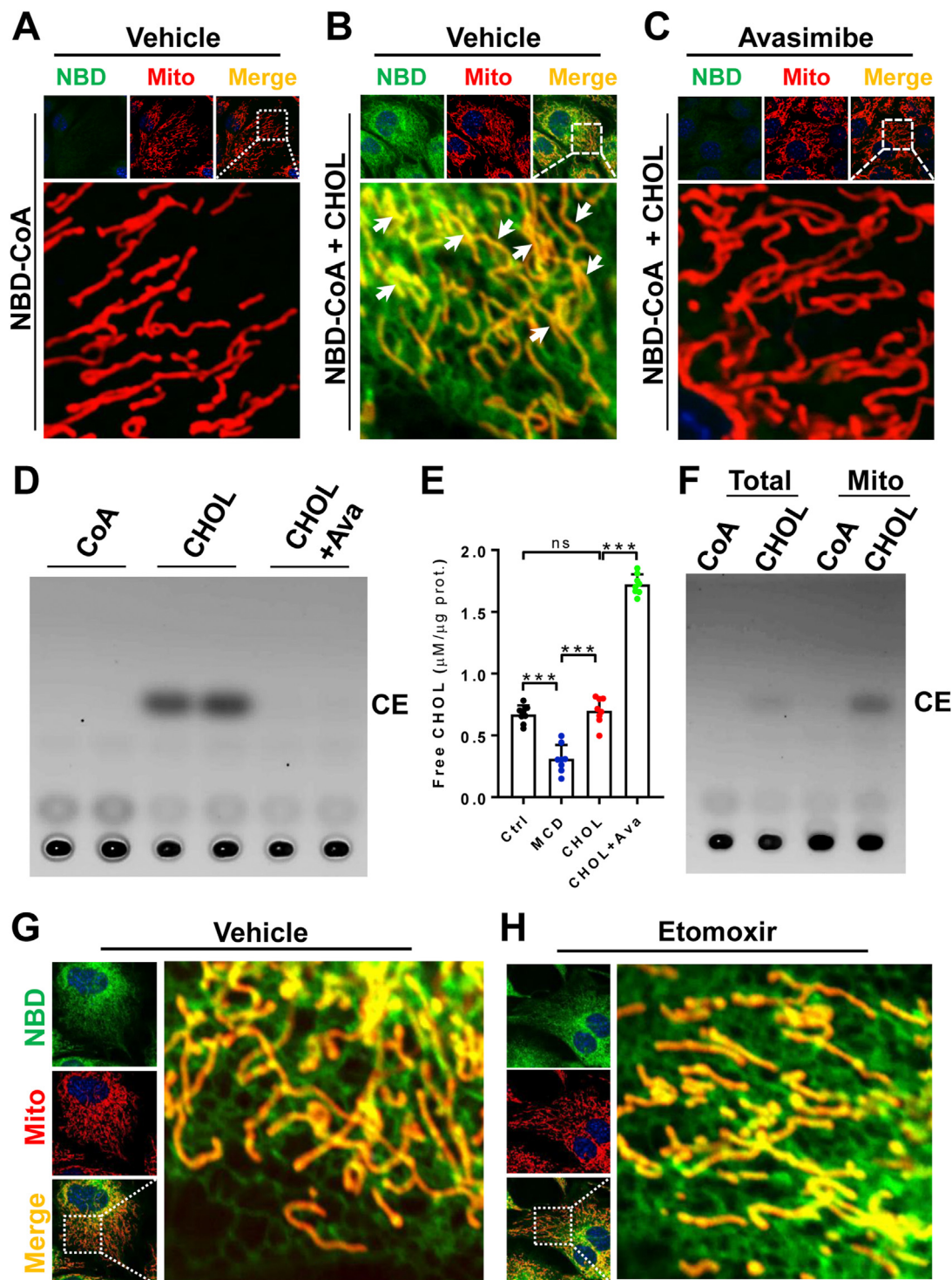
Figure 5: Labeling, confocal imaging, and TLC analysis of CE in live cells. (A-B) Confocal imaging analysis of NBD labeling and mitochondrial transport of CE in live C2C12 cells which were first depleted of endogenous cholesterol by 0.5% MCD in DMEM with 0.5% fatty acids free BSA, and then incubated with NBD-palmitoyl-CoA (1 μM) alone (**A**) or NBD-palmitoyl-CoA plus cholesterol (50 μM) (**B**) for 30 min. Mitochondria were stained with MitoTracker Red. Arrows in **B** highlight the co-localization of NBD-CE with mitochondria. (**C**) Confocal imaging analysis of cholesterol esterification in response to avasimibe treatment in live C2C12 cells which were pre-treated with avasimibe (10 μM) for 4 h, followed by depletion of cholesterol by MCD and incubation with NBD-palmitoyl-CoA and cholesterol. (**D**) TLC analysis of newly remodeled NBD-CE in C2C12 cells. Cells were treated as described in panels **A**−**C**. (**E**) Measurement of the free cholesterol in C2C12 cells. Cells were treated as described in panels **A**−**C**. The control cells were only starved in DMEM with 0.5% fatty acids free BSA. n = 8/group. (**F**) TLC analysis of newly remodeled NBD-CE in isolated mitochondria. Mitochondria were isolated from cells treated as described in panels **A** and **B**. (**G**−**H**) Confocal imaging analysis of NBD labeling and mitochondrial transport of CE in the presence (**H**) or absence (**G**) of etomoxir. MCD treated C2C12 cells were pre-treated with vehicle or etomoxir for 4 h, followed by incubation with NBD-palmitoyl-CoA plus cholesterol for 30 min. Data are representative of at least three independent experiments, and are represented as mean ± SD, ***$p < 0.001$ by one-way ANOVA.

support of the specificity of the labeling method, neither PRELID1 nor TRIAP1 deficiency had any significant effect on mitochondrial transport of newly remodeled PC (Figure 9A—C, arrows highlight the co-localization of NBD-PC with mitochondria, quantified by Pearson's correlation coefficient of mitochondria and NBD-PC in Figs. S9D and S9E).

3.3. An unexpected role of StARD7 protein in mediating mitochondrial PG transport

The StAR-related lipid transfer domain protein 7 (StARD7) is a member of the START domain-containing family of proteins, and is implicated in transport of PC between membranes [13]. Targeted deletion of StARD7 also leads to mitochondrial dysfunction and loss of mitochondrial crista, but the underlying causes remain elusive [14]. Using C2C12 cells with CRISPR-Cas9-mediated deletion of the *Stard7* gene, we investigated the role of StARD7 in mediating phospholipid trafficking between the ER and mitochondria. The knockout of *Stard7* in C2C12 cells was confirmed by qRT-PCR analysis (Figure 4D). Consistent with the reported role in PC transport, ablation of StARD7 indeed impaired mitochondrial transport of newly remodeled PC, as evidenced by a lack of co-localization of red (mitochondria) with green (PC) (Figure 4B) relative to the vector control (Figure 4A, arrows highlight the co-localization of NBD-PC with mitochondria, quantified by Pearson's correlation coefficient in Figure 4C). These results were further confirmed by TLC analysis of the kinetic profile of the mitochondrial transport of newly remodeled PC. In contrast to vector control, ablation of StARD7 significantly slowed mitochondrial transport of newly NBD-PC (Figure 10A—C). Surprisingly, StARD7 deletion also significantly impaired mitochondrial PG transport, revealing an unexpected role of StARD7 in mitochondrial PG trafficking (Figure 4E—F, arrows highlight the co-localization of NBD-PG with mitochondria, quantified by Pearson's correlation coefficient in Figure 4G). In support of the finding, StARD7 deficiency also significantly slowed down mitochondrial PG transport, leading to decreased mitochondrial NBD-PG content in StARD7 deficient cells (Figure 10D—F). In contrast, StARD7 is not required for mitochondrial PA trafficking (Figure 4H—J, arrows highlight the co-localization of NBD-PA with mitochondria).

3.4. De novo labeling of CE revealed a surprising feature of mitochondrial CE trafficking

Mitochondrial cholesterol transport plays a vital role in the synthesis of steroids, oxysterols, and hepatic bile acids [15—17]. Mitochondrial membranes are intrinsically low in cholesterol content when compared with other membranes, and therefore rely upon cholesterol transport from other organelles for steroidogenesis. The prevailing hypothesis of mitochondrial cholesterol transport is that hydrolysis of CE from LDs provides the major source for mitochondrial cholesterol transport [18]. However, it is not known whether CE can also be transported to mitochondria. The ER is the major site for cholesterol esterification, as both acyl-coenzyme A: cholesterol acyltransferase-1 and 2 (ACAT1 and ACAT2) are localized in the ER [19]. We next determined whether the *de novo* lipid labeling method can be used to label CE through acylation by ACAT enzymes, and if so, whether the newly remodeled CE can be transported from the ER to mitochondria. The results showed that addition of NBD-palmitoyl-CoA together with cholesterol to the culture medium resulted in NBD labeling of CE, as revealed by results from confocal imaging analysis (Figure 5A—B, arrows highlight the co-location of NBD-CE with mitochondria) and TLC analysis (Figure 5D). In support of the specificity of the labeling, treatment of C2C12 cells with avasimibe, a potent inhibitor of both ACAT1 and ACAT2 enzymes, completely abolished the labeling (Figure 5C—D), leading to a significant increase in total cellular free cholesterol level (Figure 5E).

Surprisingly, part of the CE was rapidly transported to mitochondria (Figure 5B, highlighted by arrows). This finding was further confirmed by TLC analysis, which showed that NBD labeled CE was only detectable in mitochondria isolated from cells incubated with both NBD-palmitoyl-CoA and cholesterol, but not NBD-palmitoyl-CoA alone (Figure 5F). To further confirm that CE, but not the NBD-labeled fatty acid from the hydrolysis of newly remodeled NBD-CE, is directly transported to mitochondria, the cells were treated with etomoxir to inhibit the carnitine palmitoyl transferase which is required for mitochondrial fatty acid uptake. The data showed that etomoxir did not significantly affect mitochondrial CE transport (Figure 5G—H). Together, these findings further confirm that the newly remodeled CE, but not NBD-labeled free fatty acids released from the CE, were indeed transported to mitochondria.

3.5. De novo labeling of TG uncovered remarkable differences between monoacylglycerol (MG) and diacylglycerol (DG) in regulating LDs biogenesis

TG, which is composed of three fatty acyl groups esterified to a glycerol backbone at the *sn-1*, *sn-2* and *sn-3* positions, and is used primarily for energy storage. Like phospholipids, TG is also subjected to remodeling after *de novo* synthesis or after digestion in the gut, which is catalyzed sequentially by monoacylglycerol acyltransferases (MGAT) and diacylglycerol acyltransferases (DGAT) [20]. Both MGAT1 and DGAT enzymes are localized at the ER, the primary site for LDs biogenesis as well [21]. We next tested whether the lipid labeling method can be used to label TG in live cells. COS-7 cells were transiently transfected with DsRed2-ER5 to label the ER, stained with BODIPY 650/665, a red fluorescent dye for TG to label existing LDs. The cells were washed with culture medium to get rid of BODIPY 650/665, followed by incubation with NBD-palmitoyl-CoA alone or together with either MG or DG as the substrates for TG remodeling. Addition of MG or DG led to NBD labeling of newly remodeled TG which was transported to LDs, suggesting that attachment of NDB did not abolish their propensity of being transported by lipid transporters (Figure 6A—B, arrows highlight the co-localization of NBD-TG with LDs). In support of the findings, the newly synthesized NBD-TG can also be detected by TLC analysis only in the presence of both NBD-palmitoyl-CoA and MG or DG, but not NBD-palmitoyl-CoA alone (Figure 6C). Furthermore, overexpression of DGAT1 in COS-7 cells significantly increased the NBD-TG formation, which was significantly inhibited by A922500, a specific inhibitor of DGAT1, as evidenced by TLC analysis (Figure 6D). Remarkably, the *de novo* labeling method revealed striking differences in subcellular distribution between newly remodeled TG from MG and those from DG. Accordingly, TG synthesized from DG were completely co-localized with BODIPY 650/665 on existing LDs. In contrast, TG synthesized from MG were still wrapped by the ER sheets, and only partially co-localized with BODIPY 650/665 on LDs (Figure 6A—B). The findings suggested that either TG synthesized from MG stimulated LDs biogenesis or they were also recruited to small LDs which exhibit poor staining by BODIPY 650/665 [22]. It is commonly believed that LDs are cytosolic organelles that are produced from the ER membrane [23]. Since only TG synthesized from MG co-stained with LDs wrapped by ER, our findings suggested that MG likely stimulated LD biogenesis. This notion is corroborated by our previous report that overexpression of MGAT1, which catalyzes TG synthesis with MG, also stimulated LDs biogenesis [24].

3.6. A striking difference between de novo remodeled lipids and exogenously labeled lipids in subcellular localizations

Exogenous fluorescence probe-labeled lipids are often used to investigate their trafficking in live cells by confocal imaging analysis
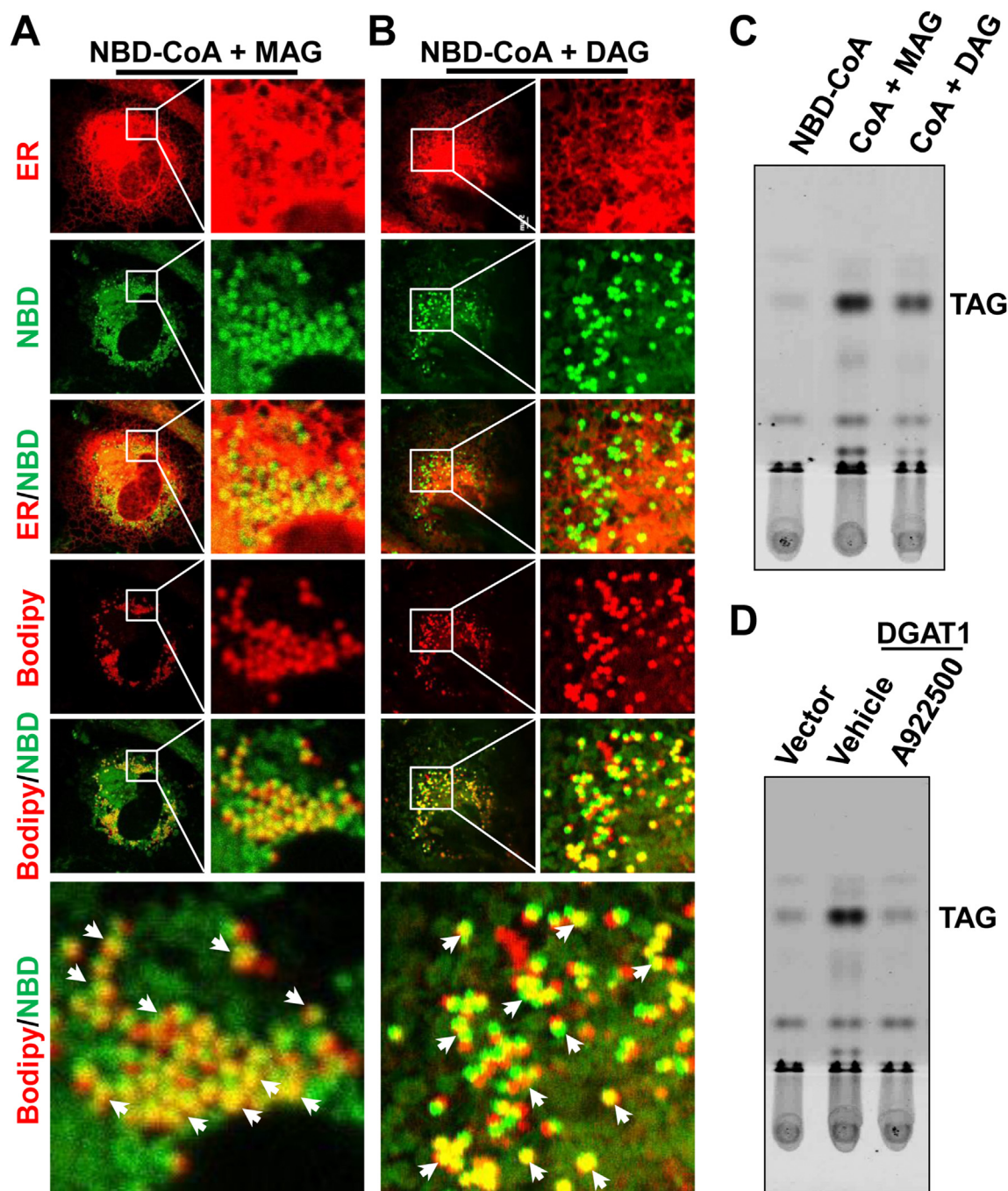
Figure 6: Labeling and confocal imaging of TG in live cells. (A) Confocal imaging analysis of COS-7 cells incubated with NBD-palmitoyl-CoA and MG. Arrows indicate the co-localization of NBD-TG with LDs. **(B)** Confocal imaging analysis of COS-7 cells incubated with NBD-palmitoyl-CoA and DG. Arrows highlight the co-localization of NBD-TG with LDs. COS-7 cells were starved in KRPH buffer containing BODIPY 650/665 to label LDs for 1 h before incubating with NBD-palmitoyl-CoA (1 μM) plus MG 18:1 (20 μM) or DG 36:2 (20 μM). The ER was visualized by transfecting cells with DsRed2-ER5. **(C)** TLC analysis of newly remodeled NBD-TG in COS-7 cells. **(D)** TLC analysis of newly remodeled NBD-TG in COS-7 cells overexpressed DGAT1 in the presence or absence of A922500 (10 μM), an inhibitor of DGAT1. Data are representative of at least three independent experiments.

[12,25,26]. However, it remains a major issue whether these exogenous fluorophore-labeled lipids are fully functional after loading into cells, since most of the exogenously labeled lipids end up in the plasma membrane and endosomes, possibly as a result of endocytosis and degradation [2]. We next investigated the subcellular localization of exogenous NBD-labeled phospholipids and cholesterol in live C2C12 cells stained with LysoTracker Red, a fluorescent dye to label

lysosomes. The results showed that these exogenous NBD-labeled lipids, including 18:1—12:0 NBD-PA, 18:1—12:0 NBD-PS, 18:1—12:0 NBD-PC, and 25-NBD-cholesterol, did not exhibit their projected subcellular localization function when compared with the *de novo* labeled lipids. In contrast to the *de novo* NBD-labeled phospholipids through the remodeling pathway, almost all the exogenous NBD-labeled phospholipids and cholesterol co-localized with lysosomes
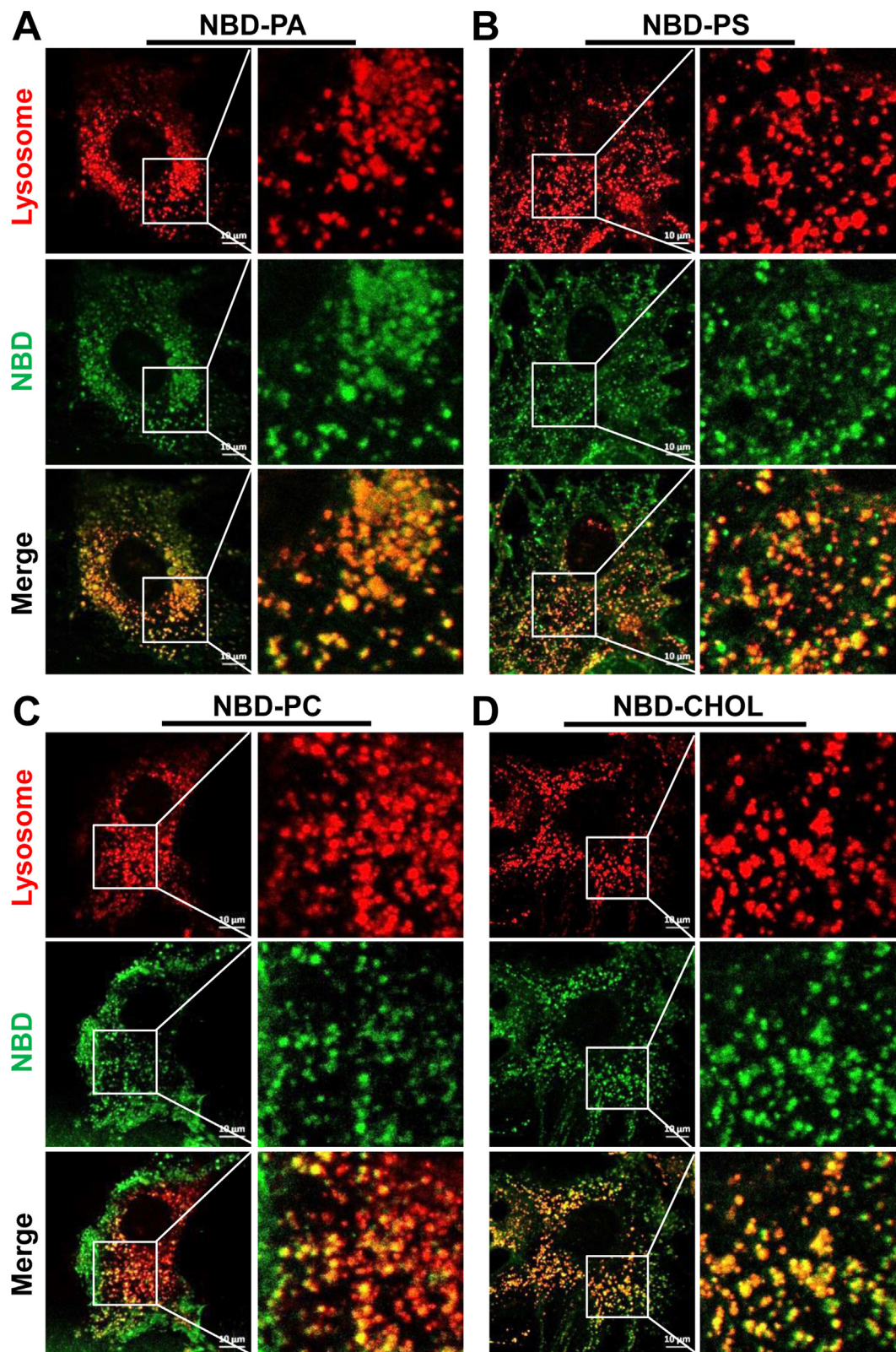
Figure 7: Subcellular localization of exogenous NBD-lipids in live cells. C2C12 cells were starved in KRPH buffer for 1 h, and then incubated with exogenous NBD-lipids (1 μM), including 18:1—12:0 NBD-PA (**A**), 18:1—12:0 NBD-PS (**B**), 18:1—12:0 NBD-PC (**C**) or 25-NBD-cholesterol (**D**). Lysosomes were stained with LysoTracker Red. Data are representative of at least three independent experiments.

(Figure 7A—D). Although the exogenous NBD-labeled lipids did not share identical acyl compositions with the *de novo* NBD-labeled lipids, nevertheless, our data suggest that these exogenous NBD-phospholipids and cholesterol are not fully functional in cells, and were primarily taken up by the lysosomes for degradation through lipophagy.

4. DISCUSSION

There are more than 1000 lipid species in a typical mammalian cell. Their level of complexity in subcellular organization and distribution within the cell is truly remarkable [27]. Although various molecular probes were developed in recent years to visualize their subcellular localization, organization, and dynamics [2], including fluorophore-labeled lipids, antibodies, toxin domains, and genetically encoded protein domains [2], none of the approaches can distinguish the acyl composition of any given lipid species *in vivo*, which is one of the most important features of a lipid. Additionally, there are many limitations with these approaches. For example, an attachment of a protein or large molecule to a lipid often disrupts its biophysical properties, leading to misplacement in subcellular distribution and a loss of function [28,29]. Additionally, nearly all the exogenously labeled lipid species failed to mimic the function of their endogenous counterparts *in vivo*, since most of the exogenously labeled lipids end up in the lysosomes, as confirmed by the current study. In this study, we have resolved these issues by developing a *de novo* lipid labeling method for individual lipid species with precise acyl composition in live cells. The method takes advantage of endogenous lipid remodeling pathways by substituting the cells with exogenous lysolipids and NBD-acyl-CoA as substrates, leading to the production of remodeled lipids with attachment of the NBD fluorescence probe. We have further demonstrated the specificity and utility of the labeling method in monitoring intracellular trafficking of major lipid species, including glycerolipids, phospholipids, and CE.

Attachment of an NBD fluorescent group to the newly remodeled lipid molecules always raises a concern whether they faithfully represent the functionality and behavior of the endogenous lipids inside a live cell. We have addressed this important issue by multiple approaches. Firstly, we demonstrated that attachment of the NBD group to acyl-CoA did not significantly affect its function as an acyl donor, since both NBD-acyl-CoA and lysolipids were recognized by the endogenous remodeling enzymes as substrates. As evidenced by results from TLC analysis, the newly remodeled NDB-labeled lipids can only be detected if both NBD-acyl-CoA and lysolipids were supplemented in the culture medium, but not NBD-acyl-CoA alone. Secondly, we showed the attachment of the NDB molecule to the newly remodeled lipid molecules did not affect their biological properties, since they were efficiently transported to subcellular localizations just like their endogenous counterparts, including mitochondria and LDs. Thirdly, using cell lines deficient in previously identified phospholipid transporters, we showed that these newly remodeled phospholipids were still recognized by the endogenous mitochondrial phospholipid transporters. Accordingly, ablation of the previously identified mitochondrial transporters prevented the mitochondrial trafficking of newly labeled NBD-phospholipids. Finally, we showed that inhibition of ACAT enzymes by avasimibe or DGAT enzyme by A922500 abolished the acylation of cholesterol and DG by NBD-acyl-CoA.

The *de novo* lipid labeling method uses relatively high concentrations of exogenous lysolipids and NBD-acyl-CoA to overcome the background from the acylation of the endogenous lysolipids, which raises other major concerns, including specificity, cellular toxicity, and further modifications of the newly remodeled lipids. We have successfully addressed all these concerns by multiple approaches. As shown by our results from cellular toxicity analysis, none of the lysophospholipids or free cholesterol caused significant cellular toxicity, which is also supported by results from western blot analysis of major biomarkers of ER stress and regulators of mitochondrial dynamics. In support of the results from cellular toxicity analysis, none of the lysophospholipids or cholesterol caused ER stress, disruption of mitochondrial dynamics, or affected mitochondrial respiration when used at the same concentrations for the *de novo* lipid labeling analysis. Additionally, we confirmed the identity and specificity of the *de novo* NBD-labeled lipids by TLC and lipidomic analysis, which showed that newly remodeled NBD-labeled lipids can only be detected if both NBD-palmitoyl-CoA and lysolipids were added to the culture medium. Consistent with these findings, no major NBD fluorescent signal was detected by confocal imaging analysis when NBD-palmitoyl-CoA alone was used for the labeling experiments, likely reflecting the low concentrations of the endogenous lysolipids. We further confirmed the specificity of the *de novo* labeled lipids by lipidomic analysis of newly remodeled PG species, which matched the acyl composition of the LPG supplemented to the culture medium. Finally, we also resolved the issue of possible further modifications of newly remodeled lipids. Although the newly remodeled lipids, such as PA, could be used as substrate for the synthesis of other phospholipids, including PC, PE, and PG, such modifications did not take place during the short *de novo* labeling time, as evidenced by results from time lapse confocal imaging and TLC analyses.

The *de novo* lipid labeling method allowed us to uncover some striking new features of lipid remodeling enzymes and transporters that were not possible by conventional biochemical assays. Accordingly, we identified a striking functional difference between TG synthesized from MG and DG. In contrast to TG synthesized from DG which were directly recruited to mature LDs, TG synthesized from MG were still wrapped by the ER, and recruited to nascent LDs, implicating a potential role of MG in stimulating LD biogenesis. This notion is corroborated by our previous report that overexpression of MGAT1, which catalyzes the acylation of MG and DG to TG, stimulated LDs biogenesis [24]. Mitochondrial cholesterol transport plays an important role in maintaining mitochondrial membrane fluidity, permeability, and respiration [17]. The prevailing hypothesis is that CE must be first hydrolyzed to free cholesterol before being transported to mitochondria for steroidogenesis [30]. Although the ER is the major site for cholesterol esterification, as both ACAT1 and ACAT2 are localized in the ER [19], it remains debated whether CEs can also be directly transported to mitochondria without hydrolysis. Using confocal imaging analysis, we resolved this issue by demonstrating that newly remodeled CEs were rapidly transported from the ER to mitochondria. The findings were supported by results from TLC analysis that CEs can only be detected in purified mitochondria if both NBD-palmitoyl-CoA and cholesterol were supplemented to the culture medium, but not NBD-palmitoyl-CoA alone. Our findings are further corroborated by previous reports that ACAT1 enzyme was predominantly expressed in steroidogenic tissues [31], and pharmacological inhibition of ACAT1 by a small molecule inhibitor significantly attenuated adrenocorticotropic hormone (ACTH)-stimulated cortisol production in an animal model of Cushing's syndrome [32].

Using stable cell lines deficient in phospholipid transporters, including TRIAP1/PRELI and StARD7, we further validated the specificity and

functionality of the *de novo* labeled phospholipids. Accordingly, we showed that ablation of TRIAP1/PRELI not only abolished their previously reported role in facilitating mitochondrial PA transport [12], but also significantly attenuated mitochondrial PG transport from the ER. The findings are indirectly corroborated by a previous report that ablation of the TRIAP1/PRELI protein complex caused apoptosis of cells, which can only be circumvented by supplementation of excessive amounts of PG [12]. Likewise, we demonstrated that in addition to a previously reported function in mediating mitochondrial PC transporter [13,33,34], StARD7 also plays a major role in facilitating mitochondrial PG transport. Our findings offered a logical explanation why depletion of StARD7 caused mitochondrial dysfunction [14], since PG is a substrate for the synthesis of CL, and CL depletion caused both mitochondrial dysfunction and a loss of crista structure [35,36]. It should be noted that the newly remodeled phospholipids exhibit a heterogeneous distribution pattern in the mitochondria. We believe that this is primarily caused by the heterogeneous nature of ER-mitochondrial contact sites, which is limited to certain region of the ER network, known as the mitochondrial associated membrane. Additionally, the mitochondrial network is quite dynamic and constantly goes through periodical cycles of fusion and fission, which could also lead to heterogeneous distribution of newly remodeled phospholipids.

Finally, the *do novo* labeling method revealed some striking differences between *de novo* labeled lipids and the exogenously labeled lipids in subcellular localization and function. In contrast to the exogenous NBD-labeled lipids which were primarily degraded through lipophagy, the *de novo* labeled lipids retained full features of the endogenous counterparts, including subcellular localization, intracellular trafficking, and biological function. Together, our findings suggest that the *de novo* lipid labeling not only provides a powerful tool for the functional analysis of individual lipid species and putative lipid transporters in live cells, but also calls for re-evaluation of previously published work involving the use of exogenously NBD labeled lipids.

AUTHOR CONTRIBUTIONS

Y.S. conceived the project and designed the research plan. J.Z., J.N., H.S., J.L. and J-P.A performed the experiments. Y.S., J.Z., J.N., H.S. J.L. and J-P.A. analyzed the data. Y.S. and J.Z. wrote the manuscript and all authors edited it.

ACKNOWLEDGEMENTS

CONFLICT OF INTERESTS

None declared.

APPENDIX A. SUPPLEMENTARY DATA

Supplementary data to this article can be found online at https://doi.org/10.1016/j.molmet.2022.101511.

REFERENCES

[1] Fahy, E., Subramaniam, S., Murphy, R.C., Nishijima, M., Raetz, C.R., Shimizu, T., et al., 2009. Update of the LIPID MAPS comprehensive classification system for lipids. Journal of Lipid Research 50(Suppl):S9—S14.

[2] Maekawa, M., Fairn, G.D., 2014. Molecular probes to visualize the location, organization and dynamics of lipids. Journal of Cell Science 127(Pt 22):4801—4812.

[3] Krishnamurthy, K., Dasgupta, S., Bieberich, E., 2007. Development and characterization of a novel anti-ceramide antibody. Journal of Lipid Research 48(4):968—975.

[4] Kleusch, C., Hersch, N., Hoffmann, B., Merkel, R., Csiszar, A., 2012. Fluorescent lipids: functional parts of fusogenic liposomes and tools for cell membrane labeling and visualization. Molecules 17(1):1055—1073.

[5] Paulusma, C.C., Houwen, R.H., Williamson, P.L., 2011. The flip side of cardiolipin import. Nature Medicine 17(4):413 author reply 413-414.

[6] Li, J., Romestaing, C., Han, X., Li, Y., Hao, X., Wu, Y., et al., 2010. Cardiolipin remodeling by ALCAT1 links oxidative stress and mitochondrial dysfunction to obesity. Cell Metabolism 12(2):154—165.

[7] Shi, Y., 2010. Emerging roles of cardiolipin remodeling in mitochondrial dysfunction associated with diabetes, obesity, and cardiovascular diseases. J Biomed Res 24(1):6—15.

[8] Zhang, J., Xu, D., Nie, J., Han, R., Zhai, Y., Shi, Y., 2014. Comparative gene identification-58 (CGI-58) promotes autophagy as a putative lysophosphatidylglycerol acyltransferase. Journal of Biological Chemistry 289(47):33044—33053.

[9] Yang, Y., Cao, J., Shi, Y., 2004. Identification and characterization of a gene encoding human LPGAT1, an endoplasmic reticulum-associated lysophosphatidylglycerol acyltransferase. Journal of Biological Chemistry 279(53):55866—55874.

[10] Bolte, S., Cordelieres, F.P., 2006. A guided tour into subcellular colocalization analysis in light microscopy. Journal of Microscopy 224(Pt 3):213—232.

[11] Wieckowski, M.R., Giorgi, C., Lebiedzinska, M., Duszynski, J., Pinton, P., 2009. Isolation of mitochondria-associated membranes and mitochondria from animal tissues and cells. Nature Protocols 4(11):1582—1590.

[12] Potting, C., Tatsuta, T., König, T., Haag, M., Wai, T., Aaltonen, M.J., et al., 2013. TRIAP1/PRELI complexes prevent apoptosis by mediating intramitochondrial transport of phosphatidic acid. Cell Metabolism 18(2):287—295.

[13] Horibata, Y., Sugimoto, H., 2010. StarD7 mediates the intracellular trafficking of phosphatidylcholine to mitochondria. Journal of Biological Chemistry 285(10):7358—7365.

[14] Saita, S., Tatsuta, T., Lampe, P.A., Konig, T., Ohba, Y., Langer, T., 2018. PARL partitions the lipid transfer protein STARD7 between the cytosol and mitochondria. The EMBO Journal 37(4).

[15] Maxfield, F.R., Wüstner, D., 2002. Intracellular cholesterol transport. Journal of Clinical Investigation 110(7):891—898.

[16] Duarte, A., Poderoso, C., Cooke, M., Soria, G., Cornejo Maciel, F., Gottifredi, V., et al., 2012. Mitochondrial fusion is essential for steroid biosynthesis. PLoS One 7(9):e45829.

[17] Andersen, J.P., Zhang, J., Sun, H., Liu, X., Liu, J., Nie, J., et al., 2020. Aster-B coordinates with Arf1 to regulate mitochondrial cholesterol transport. Molecular Metabolism 42:101055.

[18] Elustondo, P., Martin, L.A., Karten, B., 2017. Mitochondrial cholesterol import. Biochimica et Biophysica Acta (BBA) - Molecular and Cell Biology of Lipids 1862(1):90—101.

[19] Chang, T.Y., Chang, C.C., Cheng, D., 1997. Acyl-coenzyme A:cholesterol acyltransferase. Annual Review of Biochemistry 66:613—638.

[20] Shi, Y., Cheng, D., 2009. Beyond triglyceride synthesis: the dynamic functional roles of MGAT and DGAT enzymes in energy metabolism. American Journal of Physiology. Endocrinology and Metabolism 297(1):E10—E18.

[21] Robenek, H., Hofnagel, O., Buers, I., Robenek, M.J., Troyer, D., Severs, N.J., 2006. Adipophilin-enriched domains in the ER membrane are sites of lipid droplet biogenesis. Journal of Cell Science 119(Pt 20):4215—4224.

[22] Wang, H., Becuwe, M., Housden, B.E., Chitraju, C., Porras, A.J., Graham, M.M., et al., 2016. Seipin is required for converting nascent to mature lipid droplets. Elife 5.

[23] Hariri, H., Rogers, S., Ugrankar, R., Liu, Y.L., Feathers, J.R., Henne, W.M., 2018. Lipid droplet biogenesis is spatially coordinated at ER-vacuole contacts under nutritional stress. EMBO Reports 19(1):57—72.

[24] Zhang, J., Xu, D., Nie, J., Cao, J., Zhai, Y., Tong, D., et al., 2014. Mono-acylglycerol acyltransferase-2 is a tetrameric enzyme that selectively hetero-dimerizes with diacylglycerol acyltransferase-1. Journal of Biological Chemistry 289(15):10909—10918.

[25] Hailey, D.W., Rambold, A.S., Satpute-Krishnan, P., Mitra, K., Sougrat, R., Kim, P.K., et al., 2010. Mitochondria supply membranes for autophagosome biogenesis during starvation. Cell 141(4):656—667.

[26] Ray, N.B., Durairaj, L., Chen, B.B., McVerry, B.J., Ryan, A.J., Donahoe, M., et al., 2010. Dynamic regulation of cardiolipin by the lipid pump Atp8b1 de-termines the severity of lung injury in experimental pneumonia. Nature Medicine 16(10):1120—1127.

[27] Holthuis, J.C., Menon, A.K., 2014. Lipid landscapes and pipelines in mem-brane homeostasis. Nature 510(7503):48—57.

[28] Elvington, S.M., Nichols, J.W., 2007. Spontaneous, intervesicular transfer rates of fluorescent, acyl chain-labeled phosphatidylcholine analogs. Biochimica et Biophysica Acta 1768(3):502—508.

[29] Sezgin, E., Levental, I., Grzybek, M., Schwarzmann, G., Mueller, V., Honigmann, A., et al., 2012. Partitioning, diffusion, and ligand binding of raft lipid analogs in model and cellular plasma membranes. Biochimica et Bio-physica Acta 1818(7):1777—1784.

[30] Shen, W.J., Azhar, S., Kraemer, F.B., 2016. Lipid droplets and steroidogenic cells. Experimental Cell Research 340(2):209—214.

[31] Akopian, D., Medh, J.D., 2006. Genetics and molecular biology: macrophage ACAT depletion - mechanisms of atherogenesis. Current Opinion in Lipidology 17(1):85—88.

[32] Langlois, D.K., Fritz, M.C., Schall, W.D., Bari Olivier, N., Smedley, R.C., Pearson, P.G., et al., 2018. ATR-101, a selective ACAT1 inhibitor, decreases ACTH-stimulated cortisol concentrations in dogs with naturally occurring Cushing's syndrome. BMC Endocrine Disorders 18(1):24.

[33] Kanno, K., Wu, M.K., Scapa, E.F., Roderick, S.L., Cohen, D.E., 2007. Structure and function of phosphatidylcholine transfer protein (PC-TP)/StarD2. Bio-chimica et Biophysica Acta 1771(6):654—662.

[34] Kang, H.W., Wei, J., Cohen, D.E., 2010. PC-TP/StARD2: of membranes and metabolism. Trends in Endocrinology and Metabolism 21(7):449—456.

[35] Yang, Y., Cao, J., Shi, Y., 2004. Identification and characterization of a gene encoding human LPGAT1, an endoplasmic reticulum-associated lysophos-phatidylglycerol acyltransferase. Journal of Biological Chemistry 279(53): 55866—55874.

[36] Zhang, X., Zhang, J., Sun, H., Liu, X., Zheng, Y., Xu, D., et al., 2019. Defective phosphatidylglycerol remodeling causes hepatopathy, linking mitochondrial dysfunction to hepatosteatosis. Cell Mol Gastroenterol Hepatol 7(4):763—781.